Channel Structures of Gramicidin: Characterization of Succinyl Derivatives

Abstract. *Succinyl derivatives of gramicidin were tested for their ability to form channels in planar artificial lipid bilayers. Both* N-*succinyldeformylgramicidin methyl ester and charged* O-*succinylgramicidin formed channels, but the channels had markedly different sizes and lifetimes. This implies that gramicidin forms channels by end-to-end association. However, the doubly charged* N,O-*bissuccinyldeformylgramicidin was inactive, which suggests that only end-to-end association of gramicidin may result in channel formation.*

Gramicidin is a linear pentadecapeptide, HCO-L-Val-Gly-L-Ala-D-Leu-L-Ala-D-Val-L-Val-D-Val-L-Trp-D-Leu-L-Trp-D-Leu-L-Trp-D-Leu-L-Trp-NH-CH_2-CH_2OH (*1*), which forms channels in cell membranes and in artificial lipid bilayers (*2–7*). It has been proposed that a channel is formed by end-to-end dimerization of two gramicidin molecules, each in a single-stranded $\pi^6_{L,D}$-helical conformation (*8, 9*) which, because of the hydrogen-bonding pattern between turns of the helix, was renamed $\beta^6_{3,3}$ helix (*10, 11*). For structural reasons head-to-head (formyl end to formyl end) dimerization was considered most likely, and this was supported by the inactivity of deformylgramicidin and the high activity and first-order concentration dependence of the malonyl dimer [*N*,*N*′-(dideformylgramicidin) malonamide] (*9*). Tail-to-tail and head-to-tail configurations could also occur, but they were considered less probable and would be expected to have different kinetics of dimerization and lower unit channel conductances. In the case of single-stranded $\beta^6_{3,3}$ helices, the length of the channel is 25 to 30 Å and the channel diameter is 4 Å (*9, 10*).

More recently, Veatch and co-workers (*12–14*) proposed double-stranded helices for gramicidin, which could form in parallel and antiparallel orientation and might have different hydrogen-bonding registers and different numbers of residues per turn. Urry *et al.* (*15*) suggested that the related double-stranded β helices occur in organic solvents and are favored by high concentrations and elevated temperatures, but are not expected to form the dominant functional channel. To determine whether single-stranded or double-stranded β helices form the functional channel, Bamberg and co-workers (*16, 17*) synthesized and characterized terminal pyromellityl derivatives of gramicidin. *O*-Pyromellitylgramicidin formed channels only when added to both sides of the membrane, suggesting that the trivalent negatively charged pyromellityl group attached to the ethanol OH could not pass through the membrane and that the functional channel would have to be formed by either the head-to-head single-stranded β helix or the antiparallel double-stranded β helix (*16*). *N*-Pyromellityldeformylgramicidin was found to be inactive even when added to both sides of the membrane and did not form hybrid channels with *O*-pyromellityl derivatives, which essentially ruled out the double-stranded helix as forming the functional channel (*17*).

To characterize further the formation of channels by gramicidin, we synthesized and characterized succinyl derivatives of gramicidin. The succinyl group is not as polar as the pyromellityl group, so that the ends can slowly pass from one side of the membrane to the other, but it has the advantage of not requiring such a large hydration shell to dissipate the ion self-energy (*18*) and of providing a significantly greater distance between charges at the end of the channel, which could improve the possibility of observing tail-to-tail association. The structures to be considered are given in Table 1.

We report here that compounds **2** and **3** (Table 1) both formed channels in artificial membranes (but with entirely different properties) and compound **4** was inactive. Planar lipid membranes were formed as previously described (*19*) and membrane current was measured under voltage clamp. All experiments were begun at least 1 hour after the membrane had become black. Peptides were added to the bilayer bath from methanolic stock solutions. Channel parameters were calculated either by direct observation of the individual channel conductance events or from the power spectrum of the current noise produced by bilayers containing many channels (*20, 21*).

Figure 1 shows the single-channel events for structures **1**, **2**, and **3**. The channel sizes for **1** and **2** are very similar, although that for **1** is slightly larger in 1*M* cesium chloride. The channel formed by **3** is less than half as large and the kinetics of its formation are clearly different. The channel lifetimes, as observed from the single events or from the cutoff frequencies of the power spectra (Fig. 2), were in close agreement. We conclude that **3** forms channels with a much shorter lifetime than those formed by **2**.

When either **2** or **3** was added to only one side of the membrane there was a slow development of conductance (see Fig. 3). When the same compound was then added to the other side of the membrane there was a dramatic and rapid increase in the conductance, often by as much as three orders of magnitude. This increase was never observed in the case of **1** itself. Compound **4** was totally inactive at these concentrations. These effects can be explained by assuming that when either **2** or **3** is added to one side of the bilayer, its movement across the bilayer is partially restricted. Therefore the conductance increases very slowly, as most succinyl groups are located at the membrane interface on the side to which they were added. When the compound is added to the other side of the membrane, the two halves of the channel can combine. This suggests that when a succinyl group is substituted at the ethanolamine end of gramicidin the monomers form head-to-head dimers at the *N*-formyl ends. In the case of **3**, either the ethanolamine ends are able to associate by forming a tail-to-tail dimer or the succinyl ends are involved in end-to-end dimerization. The fact that the *N*,*O*-succinyl derivative is inactive suggests that only end-to-end dimers are relevant to gramicidin pore formation.

The formyl end to formyl end (head-to-head) dimerization results in six hydrogen bonds, with each end contributing three NH and three CO moieties and with a sequence of six residues, from each monomer, forming a segment with an antiparallel pleated sheet hydrogen-bonding pattern (*9*). At the ethanolamine end (the tail end) there are again three NH and three CO moieties, plus the ethanolamine OH. The oxygen of the OH, however, can form a hydrogen bond with an NH with the OH hydrogen directed

Table 1. Structures of the gramicidin derivatives.

Compound	Structural representation
1 Gramicidin	HCO——OH
2 *O*-Succinylgramicidin	$^-$OOCCH$_2$CH$_2$CO——OH
3 *N*-Succinyldeformylgramicidin	
Methyl ester, 90 percent	CH$_3$OOCCH$_2$CH$_2$CO——OH
Acid, 10 percent	HOOCCH$_2$CH$_2$CO——OH
4 *N*,*O*-Bissuccinyldeformylgramicidin	$^-$OOCCH$_2$CH$_2$CO——OOCCH$_2$CH$_2$COO$^-$

0036-8075/78/0428-0435$00.50/0

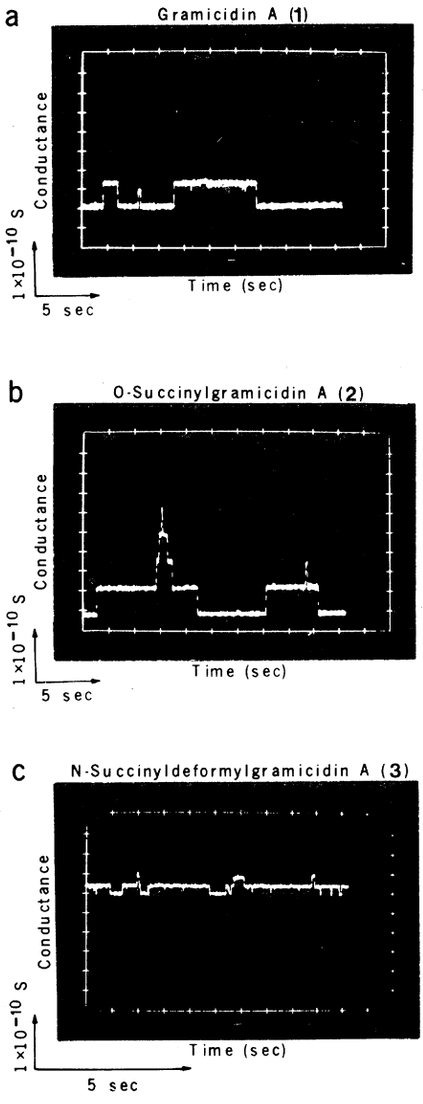

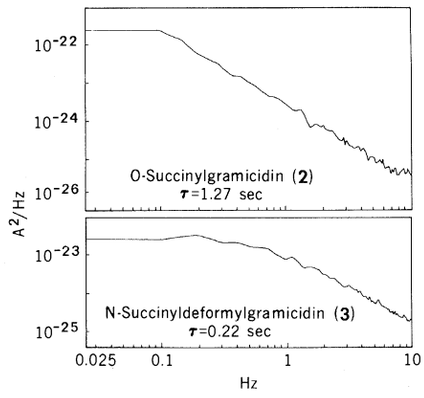

Fig. 1 (left). Single-channel conductance, in siemens (S), for gramicidin derivatives in planar artificial lipid bilayers. Membranes were formed from 2 percent (weight to volume) monoolein in *n*-decane on a 0.2-mm-diameter aperture bathed in 1*M* cesium chloride (unbuffered) at 25°C. The applied membrane voltage was 75 mV. Small amounts of compounds were added to the bath from methanolic stock solutions. Single events were recorded on a storage oscilloscope after current amplification (10^{10}) and low-pass filtering (300 Hz). The average channel sizes were as follows: gramicidin, 53 pS; *O*-succinylgramicidin, 48 pS; and *N*-succinylgramicidin, 19 pS. Fig. 2 (above). Power spectral density of bilayer current fluctuations induced by compounds **2** and **3**. Each spectrum was computed from the fast Fourier transform of 1024 points digitized from a 20-second epoch and averaged over 16 epochs. The recording conditions were as described for Fig. 1, and fewer than 100 channels were active in the membrane during data acquisition. Each averaged spectrum could be approximated by a single Lorentzian function of the form $S(f) = 2\gamma\mu\tau/[1 + (2\pi f\tau)^2]$, where f is frequency, μ is the mean conductance of the membrane, τ is the mean lifetime of the channel, and γ is the single-channel conductance.

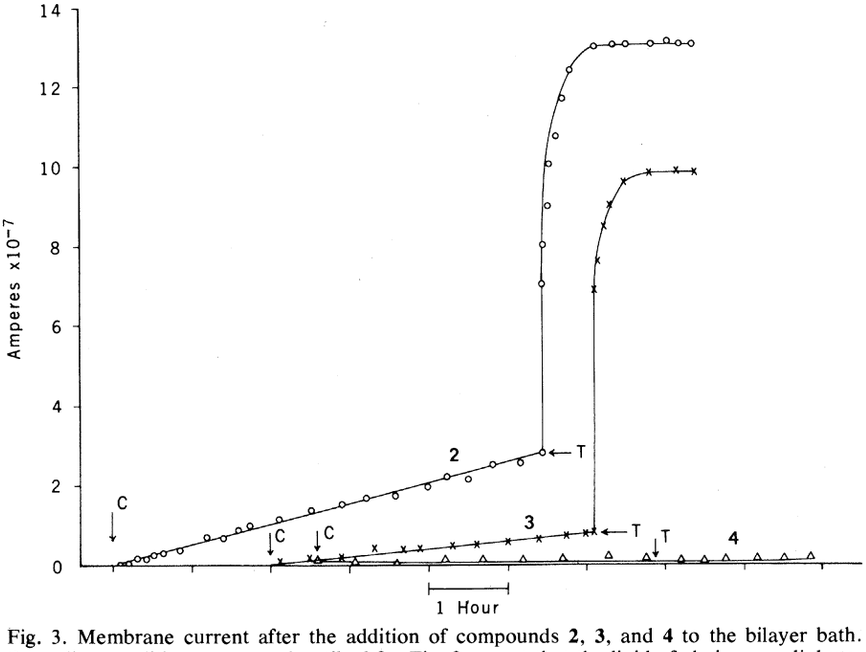

Fig. 3. Membrane current after the addition of compounds **2**, **3**, and **4** to the bilayer bath. Recording conditions were as described for Fig. 2 except that the lipid of choice was diphytanoyl L-α-lecithin, 2 percent (weight to volume) in *n*-decane. At time *C* an amount of the compound in methanolic stock solution was added to one side of the bilayer to give a concentration of 85 p*M*. At time *T* the same concentration of the compound was added to the opposite side.

outward, effectively replacing one NH. Thus there are again three hydrogen bonding protons and three CO moieties with an arrangement capable of forming six hydrogen bonds. Alternatively, head-to-head association is possible with the acid of **3** to form six hydrogen bonds, with the ester of **3** to form four hydrogen bonds, or with the acid-ester hybrid to form five hydrogen bonds. As the geometry is most favorable for association at the unmodified formyl end, the different kinetics for **3** indicate that a less stable channel is formed from end-to-end association.

With respect to the reduced unit conductance of the channel formed from **3**, it is expected that, in general, the free energy profile for a cation passing through the channel will reach a maximum in the middle of the membrane because the ion self-energy is greatest at this position (*18*), where it is most affected by the lipid dielectric constant. With the ethanolamine or the succinyl also in the middle of the membrane, the capacity of the librating peptide carbonyls to reduce the dielectric barrier would be somewhat impaired. Thus a higher barrier would occur in the middle of the membrane with end-to-end association of **3** than with head-to-head association of **1**, and **3** would form a channel with lower conductance. These results indicate that gramicidin forms dimeric channels by end-to-end association of single-stranded structures and are consistent with Bamberg *et al.* (*17*). Whether only head-to-head channels can form or whether other combinations of end-to-end channel formation can occur under some circumstances may be determined by *p*H analysis of channel formation by *N*-succinyldeformylgramicidin acid (*22*).

R. J. Bradley
Neurosciences Program, University of Alabama Medical Center, Birmingham 35294

D. W. Urry
K. Okamoto, R. Rapaka
Laboratory of Molecular Biophysics and *Cardiovascular Research and Training Center, University of Alabama Medical Center*

References and Notes

1. R. Sarges and B. Witkop, *J. Am. Chem. Soc.* **86**, 1862 (1964).
2. S. B. Hladky and D. A. Haydon, *Nature (London)* **225**, 451 (1970).
3. ———, *Biochim. Biophys. Acta* **274**, 294 (1972).
4. V. B. Myers and D. A. Haydon, *ibid.*, p. 313.
5. M. C. Goodall, *ibid.* **219**, 28 (1970).
6. S. Krasne, G. Eisenman, G. Szabo, *Science* **174**, 412 (1971).
7. E. Bamberg and P. Läuger, *J. Membr. Biol.* **11**, 177 (1973).
8. D. W. Urry, *Proc. Natl. Acad. Sci. U.S.A.* **68**, 672 (1971).
9. ———, M. C. Goodall, J. D. Glickson, D. F. Mayers, *ibid.*, p. 1907.

10. D. W. Urry, *ibid.* **69**, 1610 (1972).
11. ———, *Jerusalem Symp. Quantum Chem. Biochem.* **5**, 723 (1973).
12. W. R. Veatch, E. T. Fossel, E. R. Blout, *Biochemistry* **13**, 5249 (1974).
13. W. R. Veatch and E. R. Blout, *ibid.*, p. 5257.
14. E. T. Fossel, W. R. Veatch, Yu. A. Ovchinnikov, E. R. Blout, *ibid.*, p. 5264.
15. D. W. Urry, M. M. Long, M. Jacobs, R. D. Harris, *Ann. N.Y. Acad. Sci.* **264**, 203 (1975).
16. H. J. Apel, E. Bamberg, H. Alpes, P. Lauger, *J. Membr. Biol.* **31**, 171 (1977).
17. E. Bamberg, H. J. Apel, H. Alpes, *Proc. Natl. Acad. Sci. U.S.A.* **74**, 2402 (1977).
18. D. W. Urry, *Ann. N.Y. Acad. Sci.*, in press.
19. R. J. Bradley, W. O. Romine, M. M. Long, T. Ohnishi, M. A. Jacobs, D. W. Urry, *Arch. Biochem. Biophys.* **178**, 468 (1977).
20. H. A. Kolb, P. Lauger, E. Bamberg, *J. Membr. Biol.* **20**, 133 (1975).
21. W. O. Romine, J. Sherrette, G. B. Brown, R. J. Bradley, *Biophys. J.* **17**, 269 (1977).
22. E. Bamberg, R. J. Bradley, D. W. Urry, in preparation.
23. Supported in part by NIH grants HL-11310 and GM-07195 and NSF grant BNS75-14321. We thank E. Bamberg for very helpful discussions on the structure of **3**.

3 October 1977; revised 11 January 1978

Potassium Activation Associated with Intraneuronal Free Calcium

Abstract. *Relations between calcium entry and activation of a calcium-dependent outward current during depolarization were examined under voltage clamp in dorid giant neurons injected with the calcium-sensitive photoprotein aequorin. Activation kinetics and amplitude of the slow calcium-dependent component were both found to be related to the rate and extent of free calcium accumulation and to the electromotive force acting on potassium ions, independent of the calcium activation kinetics. This indicates that the activation of the calcium-dependent outward current is more closely related to the transient intracellular accumulation of free calcium ions than to the movement of calcium through the plasma membrane during depolarization.*

A component of outward current carried by potassium ions and activated by the entry of calcium ions through the cell surface during membrane depolarization has been inferred from recent electrophysiological studies of excitable cells (*1–7*). The calcium-sensitive late outward current $I_{K(Ca)}$ has been implicated in a number of fundamental neurophysiological phenomena including the repolarization and undershoot that follow an action potential (*3, 8*) and the hyperpolarization that follows a train of action potentials or that terminates the pacemaker wave in spontaneously bursting neurons (*9, 10*). It is distinct from the other major late potassium current, namely the classical potential-activated, delayed rectifying current $I_{K(pot)}$ (*5*). Unlike $I_{K(Ca)}$, $I_{K(pot)}$ is both insensitive to extracellular calcium-blocking agents and is blocked selectively by tetraethylammonium ions injected into the cell (*5, 7a*).

To our knowledge, activation of the calcium-dependent outward current has not, until now, been directly correlated with intracellular Ca^{2+} accumulation during depolarization of the cell membrane. A role of Ca^{2+} in the activation of this current has been inferred, however, from the following: (i) intracellular injection of Ca^{2+} can produce increase in resting conductance to K^+ (*11*); (ii) Ca^{2+} entry continues during prolonged depolarization and trains of action potentials, and K^+ conductance remains transiently enhanced following such entry (*9, 10, 12–18*), decaying as the Ca^{2+} concentration returns to the resting level (*10, 14, 15*); (iii) delayed outward current plotted against membrane voltage V_m in voltage-clamp experiments exhibits a characteristic hump that imparts an N shape to the current-voltage (*I-V*) plot (*4, 7*). The hump is eliminated by procedures that interfere with Ca^{2+} entry (*4, 5*). Formation of a hump on the late *I-V* plot has been ascribed (*4–7*) to Ca^{2+} activation of $I_{K(Ca)}$ as follows. Entry of Ca^{2+} must pass through a maximum along the voltage axis determined by the relation $I_{Ca} = g_{Ca}(V_m - E_{Ca})$, with the calcium current I_{Ca} rising with membrane voltage until the conductance g_{Ca} levels off; it undergoes a progressive decline toward zero with further displacement of the membrane potential as V_m approaches the calcium equilibrium potential E_{Ca}.

We have used the calcium-sensitive photoprotein aequorin injected into voltage-clamped neurons to examine the activation of the outward current in relation to the transient accumulation of Ca^{2+} during its entry under membrane depolarization. The Ca^{2+} concentration transient recorded during depolarization was shown to be associated with two manifestations of a calcium-dependent outward current, namely (i) the hump of the N-shaped late *I-V* plot and (ii) a component of the outward-current trajectory exhibiting slow activation kinetics (*5*). The relation of outward current activation to the Ca^{2+} signal indicates that it is not activation of g_{Ca} or I_{Ca} but rather accumulation of Ca^{2+} on its entry that determines the activation of the outward current.

Giant neurons of the nudibranch *Anisodoris nobilis* were exposed and bathed in artificial seawater containing 470 m*M* NaCl, 10 m*M* $CaCl_2$, 10 m*M* KCl, 50 m*M* $MgCl_2$, 10 m*M* glucose, and 5 m*M* Hepes [4-(2-hydroxyethyl)-1-piperazineethanesulfonic acid; Sigma] at *p*H 7.7 and 15° ± 1°C. After KCl-filled current and voltage electrodes were inserted into the cells, the aequorin dissolved in 100 m*M* KCl plus 4 m*M* 2-{[tris(hydroxymethyl)-methyl]amino}ethanesulfonic acid (Sigma) at *p*H 6.8 was slowly injected under pressure. Only cells showing normal resting and action potentials, minimal input leakage, and a minimal background aequorin emission were used. The light emitted by the injected aequorin was monitored through a fiber optic wave guide with an EMI 9635A photomultiplier tube and displayed as the aequorin signal, along with voltage and membrane current, measured at the summing junction of the operational amplifier that held the bath at ground potential. Positive-going clamp pulses lasting 200 msec were presented at 30-second intervals. Recordings were taken 30 to 180 minutes after injection of the aequorin, which allowed sufficient time for diffusion of the photoprotein throughout the neuron soma. Some characteristics of the aequorin response in these cells and details of the methods are described elsewhere (*15*). The intensity of the aequorin emission was reported to be proportional to the second or even the third power of the free Ca^{2+} concentration (*19*). Thus, to approximate the voltage-dependent transient rise in Ca^{2+} concentration near the inner surface of the membrane, we plotted the square root of the aequorin signal–voltage curve (Fig. 1B), as done by Baker *et al.* (*20*).

The amplitude of the aequorin signal at the end of the 200-msec pulse (Fig. 1A) depended on pulse voltage, reaching a maximum in different cells at potentials ranging from 30 to 70 mV (*21*) and then subsiding with further increases in potential (Fig. 1B). In the square-root plot the falling limb was linear. This behavior is predicted for the rate of entry of Ca^{2+} (see above), which lends support to the use of the square root of the aequorin signal as an approximation to the transient free Ca^{2+} concentration, $[Ca]_i$, near the cytoplasmic surface of the plasma membrane. The voltage at which the signal was fully suppressed varied in different cells, but was characteristically above 100 mV. Some cells failed to ex-

0036-8075/78/0428-0437$00.50/0